International Journal of Heat and Mass Transfer 52 (2009) 2893–2901

Contents lists available at ScienceDirect

International Journal of Heat and Mass Transfer

journal homepage: www.elsevier.com/locate/ijhmt

Radiation driven evaporation for polydisperse water sprays

William F. Godoy, Paul E. DesJardin *

Department of Mechanical and Aerospace Engineering, University at Buffalo, The State University of New York, Buffalo, NY 14260, USA

ARTICLE INFO

Article history:
Received 29 May 2008
Received in revised form 28 October 2008
Available online 21 February 2009

Keywords:
Radiation heat transfer
Water sprays evaporation
Lagrangian sectional approach

ABSTRACT

This study concerns the prediction of radiation heat transfer in evaporating water sprays for a 1D planar media. The spray evolution is described by a Lagrangian sectional approach with the initial diameter size classes defined by normal and log–normal distributions. The spray and the gas-phase radiative properties are recast in terms of cumulative distribution functions (CDF) for use with a correlated-k approach to solve the radiative transfer equation (RTE). The spectral properties required for constructing the CDFs for the droplets and gas are determined using Mie theory and the HITEMP databases, respectively. Cases are conducted to explore the sensitivity of radiative energy attenuation to time evolving droplet size distributions as a function of initial distribution, distance to the energy source, volume fraction and temperature. Results from this study show that the PDFs generate a positive skewness due to the size dependent absorption properties of the droplet. These findings suggest that the droplet size distribution can be adequately described by prescribed, non-symmetrical PDFs that are parameterized by lower order moments.

1. Introduction

The evaporation rate of water sprays is important in fire protection of highly temperature sensitive goods or in areas where water content availability is restricted as a suppression agent. Evaporation from radiation occurs immediately as the interaction of the electromagnetic waves, that carry the radiative energy, with the droplets will lead to absorption and scattering. The evolution of the droplet size distribution in time will change the attenuation of the radiative energy. Water sprays that may be initially spatially homogeneous may become inhomogeneous from radiation heat transfer alone as evaporation takes place. Although it is a fundamental problem in fire suppression, few studies have addressed droplet evaporation by radiation and further research for the optimization of thermal radiation attenuation by water sprays is necessary as pointed out by Sacadura [1] in a recent review on radiation heat transfer in fires. The main challenges due to their computational cost are: (i) solution to the RTE for a scattering media and (ii) calculation of the non-gray radiative properties of the spray.

In early work by Williams [2] analytical expressions were derived for the steady state vaporization of a single water sphere exposed to different radiant fluxes. In his work, absorption coefficients are considered constant and the energy is absorbed at a uniform rate per unit volume. Later work by Harpole [3] presents a complete analysis for the volumetric heating due to radiation absorption using a model based upon electromagnetic wave theory and ray-tracing procedures for spherical water droplets in high temperature environments. Results were presented for different diameter sizes for a single droplet as a function of time. Lage and Rangel [4,5] studied the droplet life time of n-decane and water droplets irradiated by a blackbody at 850 K and 2000 K, assuming spherical symmetric conditions. They concluded that radiation heat transfer can be as important as the choice of the liquid-phase droplet model and that the spatial non-uniformity of the imposed radiation has little effect on the overall droplet evaporation time. This fact has been studied more recently by Miliauskas [6–8] and Dombrovsky [9] for interaction of radiation and conduction processes in evaporating droplets. Dombrovsky used Mie theory for his calculations and concluded that thermal radiation is absorbed mainly in the central zone of the droplets for semi-transparent ranges and at the surface of the droplet for absorbing peaks. More recently, Tseng and Viskanta [10] developed a radiative transfer model based on geometrical optics theory, rather than Mie theory, and the solution of the radiative transfer equation inside the droplet including internal circulation to account for temperature non-uniformity. They found that the absorption of radiative energy is important for droplets larger than 100 μm for high temperatures in fire environments considering diffusion processes are dominant.

In the present work, a model is developed to account for the overall radiative attenuation of an evaporating spray in a 1D domain. The initial droplet size probability density function (PDF) is represented by either a log–normal or normal distributions that are typically found in fire suppression systems [11]. The droplet size distribution is tracked in diameter space using a Lagrangian sectional approach [12]. The spectral properties for the water

* Corresponding author. Tel.: +1 716 645 2593x2314; fax: +1 716 645 3875.
E-mail address: ped3@buffalo.edu (P.E. DesJardin).

0017-9310/$ - see front matter © 2008 Elsevier Ltd. All rights reserved.
doi:10.1016/j.ijheatmasstransfer.2008.12.005

droplets and water vapor are obtained using Mie theory [13,14] and the HITEMP database [15], respectively. A narrow band correlated-k method is used to account for the RTE solution on a non-gray basis of the medium composed of produced water vapor and liquid droplets as explained by Modest and Riazzi [16] and Wang and Modest [17]. The RTE is solved using a first order spatial discretization scheme [18] and a S_8 quadrature for the angular discretization [19]. The droplets are irradiated by a diffuse blackbody slab at a prescribed temperature as the source of radiative energy. As evaporation takes place the medium becomes non-homogeneous from spatially non-uniform heat absorption processes requiring the solution of the RTE at every time step. Results are presented for the evolution of the droplets sizes and the heat flux at different times and locations. The strength of this unique modeling description is that the PDF evolution of droplet size from radiation is treated exactly without approximations for either the evolution of the PDF or for the radiation heat transfer in the scattering media. All the codes employed for the present work has been in-house tested and validated with experimental and numerical data in a previous work by the authors [20]. To the authors' knowledge such an approach has not been previously explored for radiation driven evaporation.

2. Mathematical formulation

2.1. Radiative transfer equation (RTE) and radiative properties of water sprays

The problem under investigation is radiation heat transfer in one-dimensional planar media subject to a heat flux from a black body at one of the boundaries. The temperature inside the droplet and the produced water vapor is assumed uniform and constant. All thermo-physical properties are also assumed constant. The media composed of the evaporating spray and the gas phase resulting from this evaporation is always considered as dilute [3] therefore conduction and convection mechanisms are neglected as the main focus of this study are radiation effects. This is perfectly justified as the concentrations for the water vapor are always small as will be shown in the results.

Radiative properties required for the integration of the RTE for a scattering, absorbing and emitting media is given by [21]:

$$\vec{s}\cdot\nabla I_\lambda = k_\lambda I_{b\lambda}(T) - \beta_\lambda I_\lambda + \sigma_\lambda \frac{1}{4\pi}\int_{4\pi} I_\lambda \Phi_\lambda(\vec{s}',\vec{s})d\Omega' \quad (1)$$

where I_λ is the spectral radiative intensity which depends on the path-length (s), absorption (k_λ), scattering (σ_λ) and total extinction ($\beta_\lambda = k_\lambda + \sigma_\lambda$) coefficients along with the scattering phase function (Φ_λ). The quantity $I_{b\lambda}$ is the blackbody intensity and depends on temperature. The spectral properties for the water droplets and water vapor are obtained from Mie theory [13,14] and the HITEMP database [15], respectively. A narrow band correlated-k distribution formulation is used from the work of by Modest and Riazzi [16] and Wang and Modest [17] for 242 bands for which initially a Lorentz profile had been employed to determine the spectral values of k from HITEMP. The narrow band k-distribution values of the gas are then obtained at atmospheric pressure for 23 temperatures and 5 different concentrations for water vapor using 10 Gaussian points for each narrow band as in [16]. This procedure was employed and tested in a previous work by the authors for spectral and total solution of the RTE for water sprays [20]. Expressions for the radiative coefficients are given by Mie theory that describes the scattering and absorption of electromagnetic waves in spherical droplets [21,22]. Two physical properties govern the spectral absorption and scattering by a single particle: the size parameter $x = \pi D/\lambda$ (D is the diameter of the droplet and λ the wavelength) and the complex index of refraction $m = n - ik$ (n is the refractive index and k the absorptive index). The optical constants, n and k, for water are obtained from the work of Hale and Querry [23]. The rates of absorption and scattering by a single sphere are given in terms of efficiency factors for the total extinction, Q_{ext}, scattering, Q_{sca}, and absorption, Q_{abs}. These factors are determined from Wiscombe's work on Mie scattering calculations [14] using Lentz's method of continued fractions for Bessel functions [13]. This was adapted to an in-house code that was tested and validated by the authors in a previous study [20]. Fig. 1(a) shows the behavior of the absorption efficiency factor for a single water droplet. The water droplets are nearly transparent for wavelengths less than 2 μm. Fig.1(b) shows a closer examination of the absorption distribution as a function of the size parameters for wavelengths near peak blackbody emission for $T = 1200$ K and 1000 K, respectively. For $\lambda \simeq 2.7$ μm and 6.3 μm, the absorption increases with decreasing size (up to $x = 2$ μm), due to the strong vibrational–rotational bands of water at these wavelengths. However, for other wavelengths the absorption is shown to decrease monotonically. As will be shown in the results, this distribution is important for radiative driven droplet evaporation because, on average, the droplets will

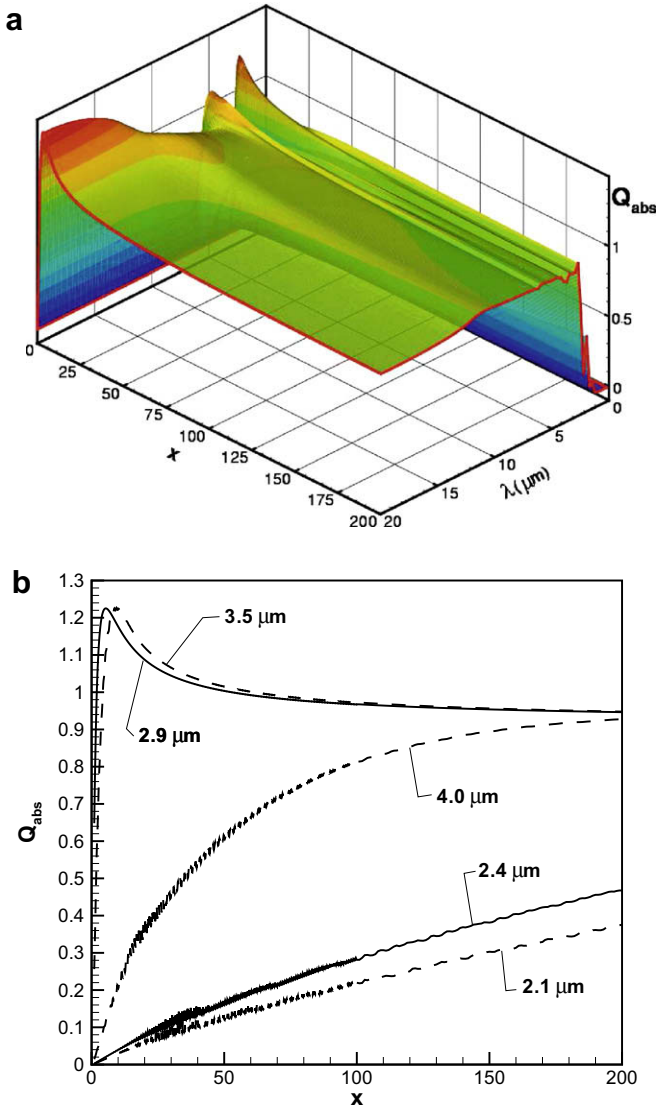

Fig. 1. Results for the absorption efficiency factor, Q_{abs} for water droplets using Mie theory for (a) as a function of size parameter x and wavelength λ and (b) detailed behavior of Q_{abs} for wavelengths near 2.4 μm and 2.9 μm (solid lines) corresponding to blackbody peak emission at 1200 K and 1000 K, respectively.

absorb less energy as they decrease in size causing a skewness in the PDF.

For water sprays, the radiative properties, R_λ ($=\{\beta_\lambda, \sigma_\lambda, k_\lambda\}$) are determined by averaging over the droplet distribution using corresponding efficiency factors Q ($=\{Q_{ext}, Q_{sca}, Q_{abs}\}$) and the droplet diameter PDF, $n(D)$ [21]:

$$R_\lambda = N_T \int_0^\infty Q(x,m)\frac{\pi D^2}{4} n(D)dD \tag{2}$$

$$\Phi_{T,\lambda} = \frac{1}{\sigma_\lambda}\int_0^\infty Q_{sca}(x,m)\Phi(x,m)\frac{\pi D^2}{4} n(D)dD \tag{3}$$

where N_T in Eq. (2) is the droplet number density and is related to the droplet volume fraction (f_v) as, $N_T = f_v/(\int_0^\infty \frac{\pi D^3}{6} n(D)dD)$ where f_v is specified.

2.2. Spray evaporation formulation using the Lagrangian sectional method

A Lagrangian modeling approach is pursued for which the droplet size distribution at each cell (Fig. 2) is decomposed into sections as illustrated in Fig. 3. An evolution for each bin diameter is constructed by considering the overall balance of energy lost from radiation and that deposited into the droplets, as shown in Fig. 2 for the problem configuration. The decrease in radiation energy from absorption is given by the contribution to the heat flux divergence,

$$\frac{dq(s)}{ds} = \int_0^\infty k_\lambda(4\pi I_{b\lambda}(T) - G_\lambda)d\lambda = \int_0^\infty \int_0^\infty N_T \frac{\pi D^2}{4} n(D) Q_{abs}(4\pi I_{b\lambda}(T) - G_\lambda)dDd\lambda \tag{4}$$

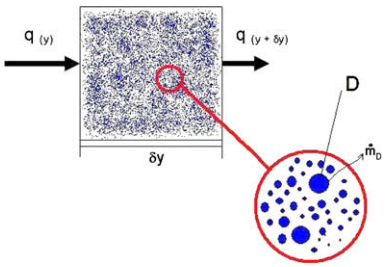

Fig. 2. Problem configuration showing the variation of the heat flux due to absorption by the water droplets and later evaporation.

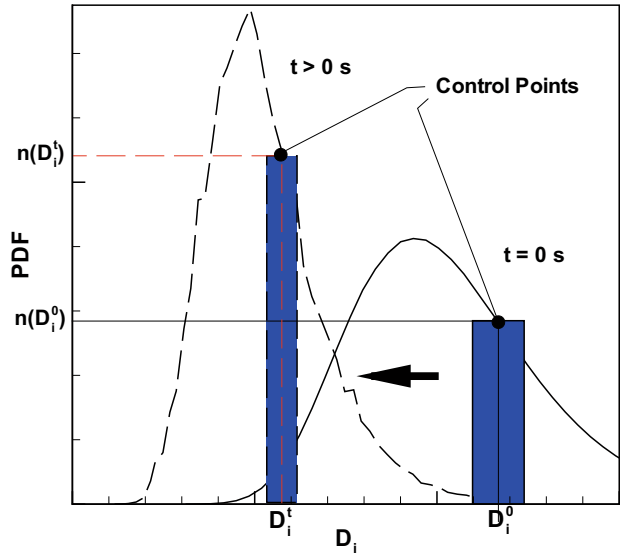

Fig. 3. Sketch of Lagrangian class decomposition of the droplet size PDF.

where G_λ is the spectral irradiation given as: $G_\lambda = \int_{4\pi} I_\lambda d\Omega'$. Neglecting the sensible internal heating of the droplet, the energy absorbed by the spray, ΔE_{evap}, is assumed to only evaporate the droplet,

$$\Delta E_{evap} = h_{fg}\int_0^\infty N_T \frac{dm_D}{dt} n(D)dD = h_{fg}\int_0^\infty N_T \rho_l \frac{\pi D^2}{2}\frac{dD}{dt} n(D)dD \tag{5}$$

where h_{fg} is the latent heat of vaporization of water, m_D is the mass for each droplet and ρ_l is the liquid water density.

Eqs. (4) and (5) and switching the order of integration in Eq. (4) results in an evolution equation for each droplet section,

$$\frac{dD}{dt} = \frac{1}{2\rho_l h_{fg}}\int_0^\infty Q_{abs}(4\pi I_{b\lambda} - G_\lambda)d\lambda \tag{6}$$

resulting in a formulation similar to that used by Barret and Clement [24] for gray media. In the present study, the non-gray behavior of the media is taken into account through the spectrally dependent absorption efficiency factor, Q_{abs}.

The diameter evolution in Eq. (6) is later applied to update the volume fraction of the droplets and the gas phase at each time step. Assuming that the droplets never reach total evaporation, as in Fig. 1 Q_{abs} decreases with the droplet diameter, the number of droplets per unit volume (N_T) remains unchanged therefore the droplet concentration is given as a function of the PDF at any time step,

$$f_{v-liq}^{t+1} = N_T \int_0^\infty \frac{\pi D^3}{6} n(D)^{t+1} dD \tag{7}$$

where f_{v-liq}^{t+1} and $n(D)^{t+1}$ are the volume fraction and the droplet PDF for a single location at a time step, respectively. The water vapor concentration is calculated from Eq. (7) assuming that only evaporation from the liquid phase contributes to increase its concentration. Therefore,

$$f_{v-wv}^{t+1} = f_{v-wv}^{t} + \left(f_{v-liq}^{t} - f_{v-liq}^{t+1}\right)\frac{\rho_{wv}}{\rho_{liq}} \tag{8}$$

where f_{v-wv}^{t+1} is the volume fraction of the water vapor for a single location at a time step, f_{v-wv}^{t}, f_{v-liq}^{t} are the volume fractions of the water vapor and liquid phase for that location at a previous time and ρ_{wv} and ρ_{liq} are the density of the water vapor and the liquid phase, respectively. Pressure and temperature remain constant therefore an expansion process occurs and it must be assumed that the droplets are diluted in the water vapor–air mixture so the equations of motion can be omitted in the analysis without introducing large errors in the calculation. Concentrations used in this study of initial $f_{v-liq} = 1\times10^{-5}$ and $f_{v-liq} = 1\times10^{-4}$ result in total water vapor concentrations of $f_{v-wv} = 1.67\%$ and $f_{v-wv} = 16.67\%$ and total volume expansions of 0.83% and 8.3% of the original volume, respectively. These values suggest that neglecting the equations of motion introduce some small error for the extreme case of high water droplets concentrations being almost negligible for most of the cases used in this study where $f_{v-liq} = 1\times10^{-5}$.

3. Numerical solution

The initial spray droplet sizes are prescribed using either normal (Gaussian) or log–normal distributions given by,

$$n(D)_{norm} = \frac{1}{\sigma_D\sqrt{2\pi}} exp\left[-\frac{(D-\bar{D})^2}{2\sigma_D^2}\right] \tag{9a}$$

$$n(D)_{log-norm} = \frac{1}{DS\sqrt{2\pi}} exp\left[\frac{-[ln(D/M)]^2}{2S^2}\right] \tag{9b}$$

where $\bar{D}$ and σ_D are the mean and root mean square, RMS, droplet diameter of the normal distribution and the parameters M and S in

the log–normal distribution are related to $\bar{D}$ and σ_D through the following relations.

$$M = \frac{\bar{D}}{\sqrt{\frac{\sigma^2}{\bar{D}^2}+1}} \tag{10a}$$

$$S = \sqrt{ln\left(\frac{\sigma^2}{\bar{D}^2}+1\right)} \tag{10b}$$

The initial droplet size distributions are discretized using evenly spaced increments with mean value D_i and height $n_i = n(D_i)$ as illustrated in Fig. 3. The area of each section represents probability that does not change with time since droplet–droplet interactions (i.e., coalescence and breakup) are not considered. Control points are defined at the center of each bin for all bins except the two located at the extreme. For the first and last bin the control points are defined as the lower and upper extremes of the distribution, respectively. With these definitions the probability of each interior bin is defined as: $P_i = n_i \Delta D_i$ where $D_i = (D_{i+1} - D_{i-1})/2$. Future values of n_i can then be determined from knowing that P_i is a constant for each bin, i.e., $n_i = P_i/\Delta D_i$.

The evolution equation for each control point is given by Eq. (6) with D replaced with D_i resulting in a system of N transport equations where N is the total number of bins. These equations are integrated in time using a first order accurate Euler method, $D_i^{n+1} = D_i^n + S_i \Delta t$ where S_i is the right-hand side of Eq. (6).

G_λ in Eq. (6) is calculated from the intensity field which is solved for using a discrete ordinates method (DOM). A S_8 quadrature with a 1 cm first order spatial discretization is used in this study from an in-house built code. We found that the spacing of 1 cm is sufficient to resolve the high absorption bands of water vapor at 2.7 μm and 6.3 μm. Fig. 4 shows the values of the mean spectral absorption coefficient that drives the heat flux along the media for the cases used in this study if total evaporation occurs for water droplet concentrations of $f_v = 1 \times 10^{-5}$ and $f_v = 1 \times 10^{-4}$ resulting in water vapor concentrations of $f_v = 1.67\%$ and $f_v = 16.67\%$, respectively. The idea of using a correlated-k method combined with a first order discretization is to provide stability to the solution by eliminating the peaks at the strong bands of water vapor as they only represent a very small fraction of the spectrum therefore the total heat flux is not altered. Overall, the code has been tested and validated for 1D media in a previous study [20]. The same procedure was applied by Kumar et al. [18] for 1D media comparing different quadratures.

The time step for integration of Eq. (6) is calculated dynamically such that $\Delta_t < min[D_i^n/|S_i(D^n)|]$. This method results in a stable solution for an arbitrary selection of N. Figs. 5 and 6 show simulation sensitivity to the time step selection and number of bins, respectively. Fig. 5 shows results comparing the use of a fixed time step of 0.10 and 0.05 seconds (s), and also using a dynamical time step. As shown, for (a) 100 bins and (b) 200 bins, fixed time steps introduce non-physical numerical instability oscillations. The finer the bin size, the greater the oscillations. Reducing the time step, reduces the oscillations but also increases the numerical cost. The use of the dynamical time step procedure eliminates this problem and recovers some of the computational time. To explore the sensitivity to the number of bins, Fig. 6 shows results for 10, 30 and 100 bins using dynamical time stepping. The results are shown to be bin number independent beyond 30 bins therefore all cases presented in the results use 30 bins.

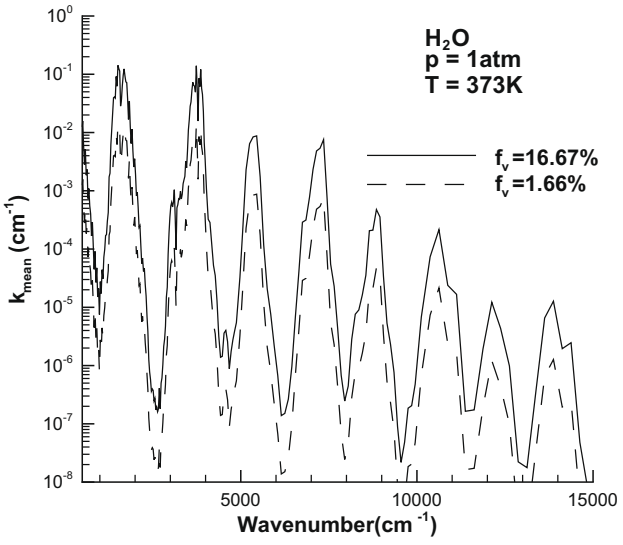

Fig. 4. Mean spectral absorption coefficient for water vapor at atmospheric pressure and $T = 373$ K for $f_v = 1.6\%$ and $f_v = 16.67\%$ corresponding to water droplets concentrations of $f_v = 1 \times 10^{-5}$ and $f_v = 1 \times 10^{-4}$, respectively.

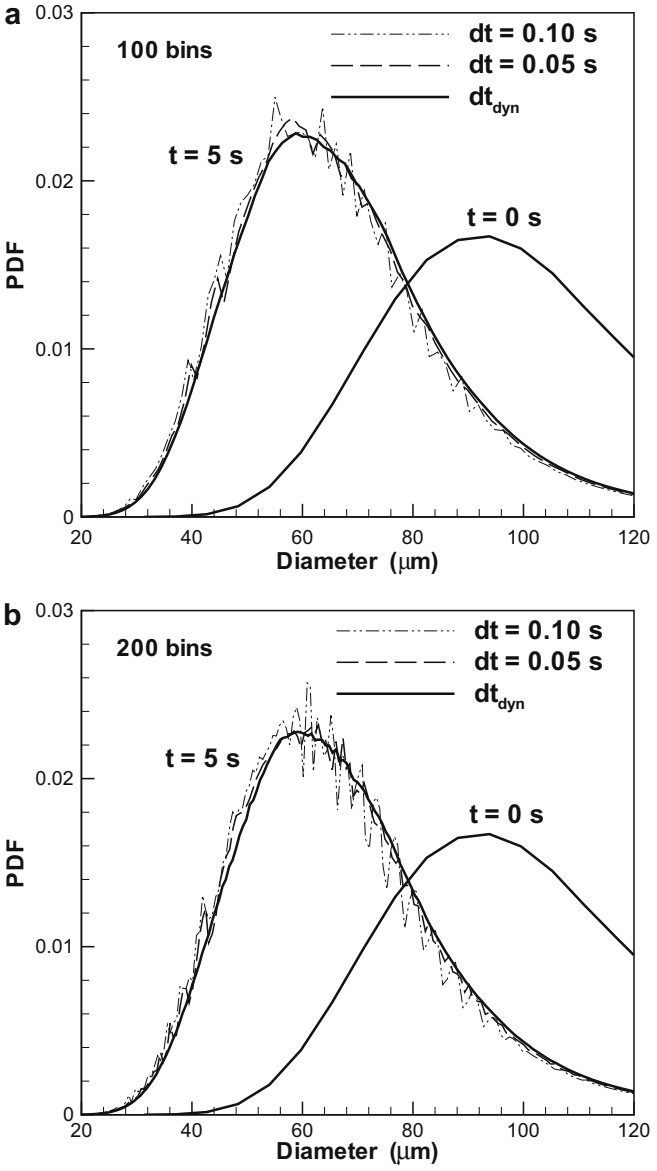

Fig. 5. Numerical stability analysis at $t = 5$ s as a function of the number of diameter size bins for (a) 100 bins and (b) 200 bins.

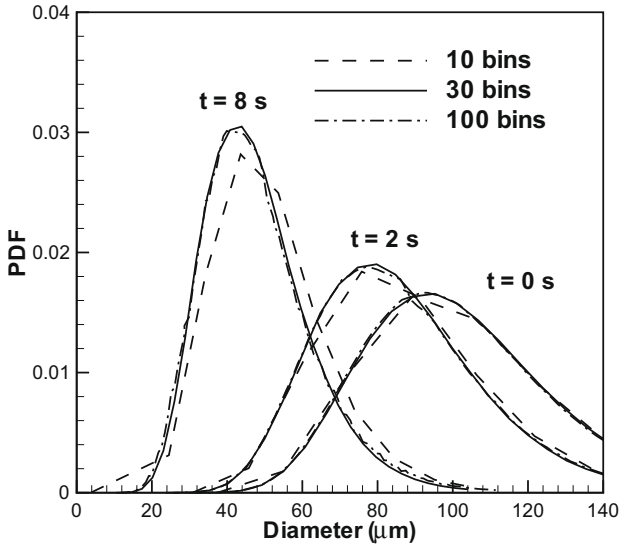

Fig. 6. Convergence analysis for different number of bins and dynamical time step at different times of the spray evaporation process.

4. Results

The problem of interest is a one-dimensional spray of total length $L_T = 100$ cm subject to a diffuse black body heat flux with temperatures of 1200 K and 1000 K. In all cases the variable L is used to describe the distance of any point of the domain to the wall, whereas x is reserved to represent the size parameter. The temperature of the droplets and gas are set equal to the boiling temperature of water at standard atmosphere of $T_m = 373$ K. The density of the water vapor and liquid are assumed to be 0.6 kg/m^3 and 1000 kg/m^3, respectively. The heat of evaporation is taken as 2270 kJ/kg. The initial droplet size PDF is assumed to follow either a log–normal or normal distribution with a prescribed arithmetic means of $M = 500$ μm, 100 μm and 50 μm with a normalized variance of $S = 0.25$ and volume loadings of $f_v = 1 \times 10^{-5}$ and 1×10^{-4}.

The simulation results are organized into four groups to study the effects of initial droplet size, wall temperature, loading and shape of the PDF (i.e., log–normal and normal). For each case, results are presented showing the (a) the droplet PDF evolution, (b) the heat flux ($\vec{q}(s) = \int_0^\infty \int_{4\pi} I_\lambda \vec{s} d\Omega' d\lambda$) and (c) heat flux divergence. For the last set of results the lower moments of the PDF are also provided (i.e., mean, RMS and skewness).

Figs. 7–9 summarize the cases for $M = 500$, 100 and 50 μm, respectively. For these cases, the wall temperature is set to 1200 K and the initial loading is $f_v = 1 \times 10^{-5}$. Results are plotted for $t = 0$ s, 2 s, 6 s, 8 s and 16 s corresponding to $L = 0$ cm (solid line) and at 100 cm (dashed line). For the largest drop case of Fig. 7, the PDF simply translates to smaller droplet sizes up to until the last time of 16 s. Based on the initial value of M, an estimated mean size parameter, x_{mean} $(= \pi M/\lambda_{max-I})$ of the spray is calculated to be 655 where $\lambda_{I-max} = 2.4$ μm is the wavelength corresponding to the peak black body emission at $T = 1200$ K. As shown in Fig. 1(a), the Q_{abs} is well beyond the constant region for $x > 655$ and therefore each bin will absorb equally, resulting in the observed translation of the PDF. After 16 s a greater portion of drops fall below $x < 25$ where Q_{abs} drops off more rapidly (see Fig. 1(b)) resulting in a rapid increase in probability for these droplets. Fig. 7(b) and (c) show that the media is radiatively thin with an initial average optical thickness of 0.12, resulting in a nearly constant heat flux and energy absorbed over the length of the domain.

Figs. 8 and 9 summarize the cases for $M = 100$ and 50 μm, respectively. The initial mean size parameters for these cases are much smaller with $x_{mean} = 131$ and 65, respectively. For these cases, the PDF becomes asymmetrical much earlier in time forming a tail for larger droplet sizes due to the non-uniform absorption of

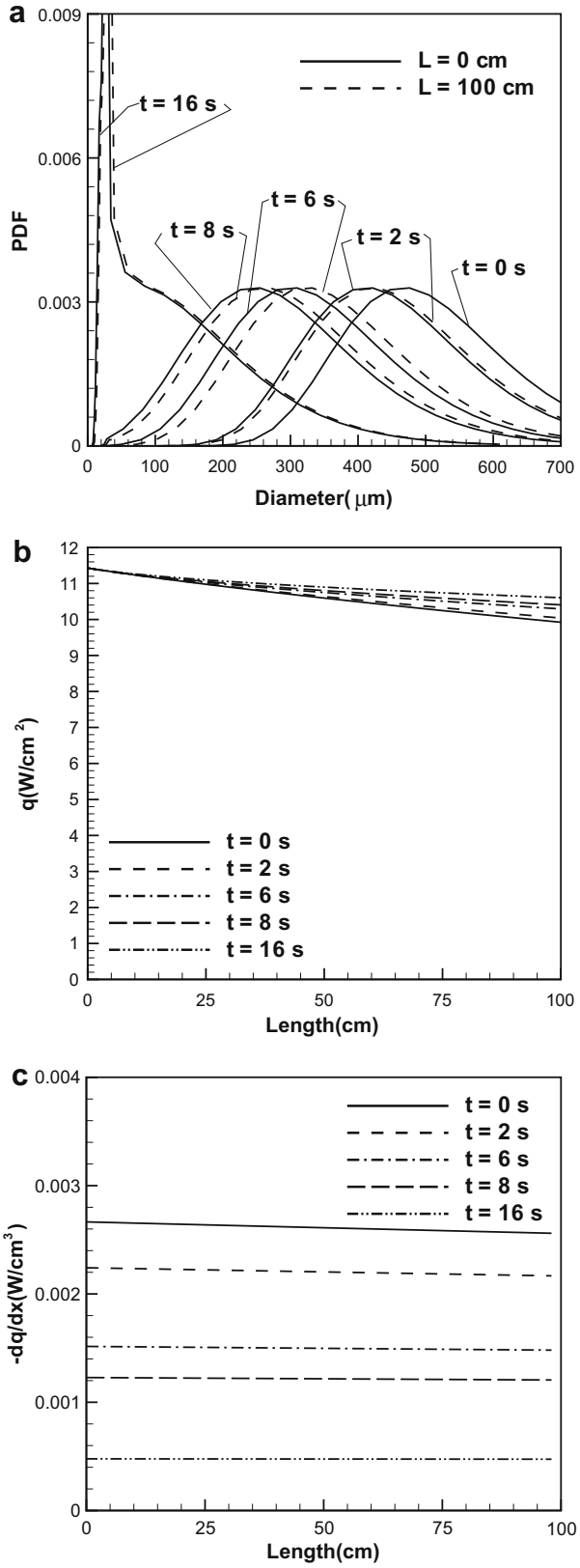

Fig. 7. Time evolution of (a) droplet size PDF, (b) radiative heat flux and (c) divergence of the radiative heat flux at $t = 0$ s, 2 s, 6 s, 8 s and 16 s for case $M = 500$ μm, $f_v = 10^{-5}$ and $T_{wall} = 1200$ K.

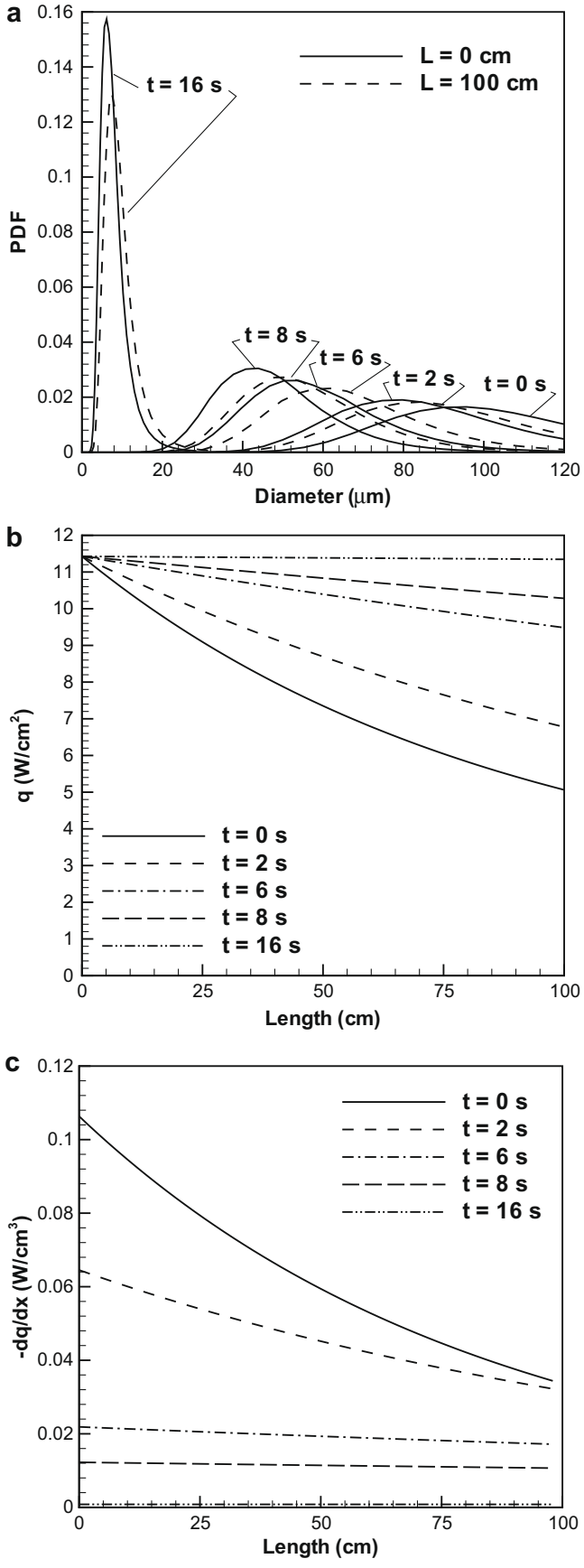

Fig. 8. Time evolution of (a) droplet size PDF, (b) radiative heat flux and (c) divergence of the radiative heat flux at $t = 0$ s, 2 s, 6 s, 8 s and 16 s for case $M = 100$ μm, $f_v = 10^{-5}$ and $T_{wall} = 1200$ K.

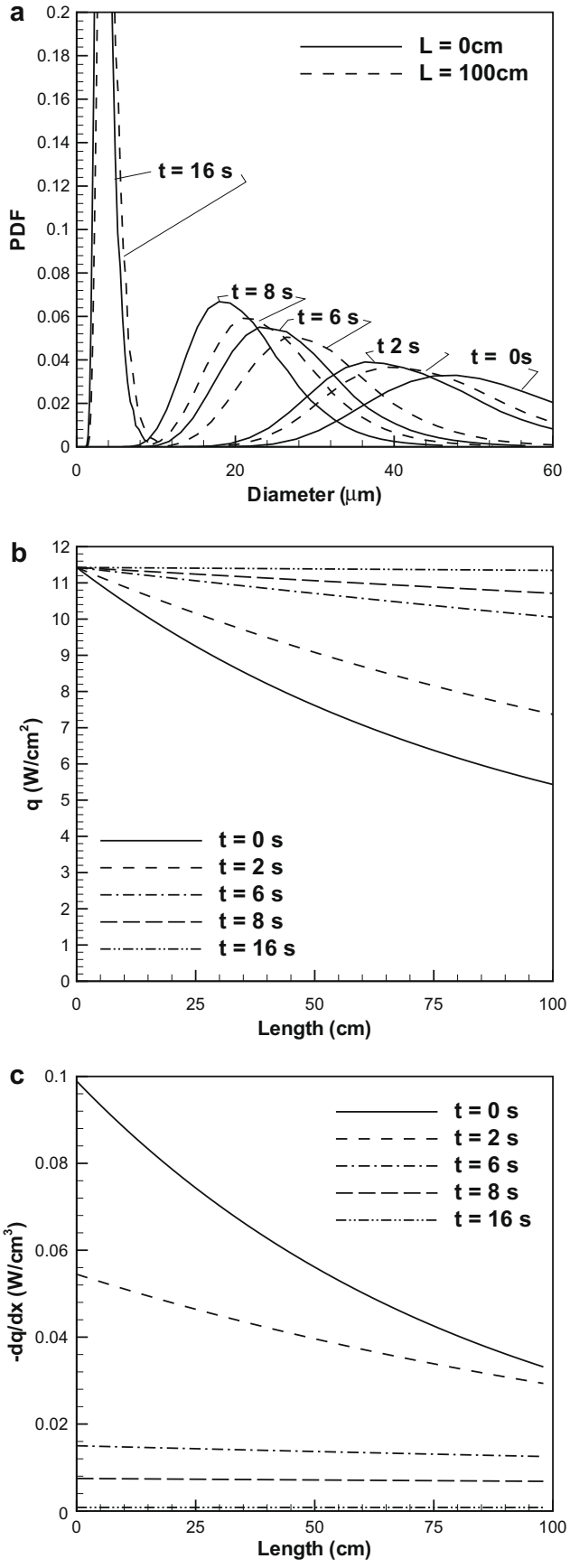

Fig. 9. Time evolution of (a) droplet size PDF, (b) radiative heat flux and (c) divergence of the radiative heat flux at $t = 0$ s, 2 s, 6 s, 8 s and 16 s for case $M = 50$ μm, $f_v = 10^{-5}$ and $T_{wall} = 1200$ K.

the water. With smaller droplets, the overall spray absorption is expected to increase due to the increase in surface to volume (i.e., an increase in the number density) for a fixed loading. This expectation is consistent with the factor of five decrease in heat flux when comparing Fig. 8(b) to 7(b) and a corresponding increase in average optical thickness to 0.784. However, a further reduction in M from 100 μm to 50 μm results in nearly the same heat flux distribution. In this case, the increase in number particle density is more than compensated by a decrease in the absorption coefficient, resulting in an average optical thickness of 0.747. Close comparison of Figs. 8(c) and 9(c) shows that 20% *more* energy is absorbed for $M = 100$ μm than for 50 μm early in time. This finding indicates that conventional wisdom of smaller droplets being more effective at absorbing radiation may not always hold true and there may be an optimal droplet size distribution for radiation driven evaporation.

Fig. 10 shows the influence of the wall temperature for the $M = 100$ μm case. In this case, the wall temperature is lowered by 17% to $T_w = 1000$ K. At this lower temperature the corresponding wavelength for peak emission is 2.9 μm. Although this wavelength is located near the strong absorbing band of the water molecule at 2.7 μm, the overall spray absorption rate decreases in time. This is shown in Fig. 10(a) in which the droplet distribution still develops a positive skewness. Overall evaporation rates are lower compared to the higher temperature case due to a decrease in the energy from the source. A 20% reduction in temperature results in a relatively large 57% decrease in the total heat flux at the emitting surface due to the fourth power dependence of emission on temperature, as shown in Fig. 10(b). The energy absorbed shown in Fig. 10(c) is also reduced as the medium evaporates at slower rates, but is qualitatively to the previous higher temperature case of Fig. 8(c).

Fig. 11 shows the influence of loading with f_v increased to 1×10^{-4} for the $M = 100$ μm baseline case. Increasing f_v results in an increase in the total number of droplets and hence more absorption by the medium. As shown in Fig. 11(b), the heat flux is 60% lower than the previous case of $f_v = 1 \times 10^{-5}$ due to a 10 times increase in the number density. The result is a decrease in the evaporation rate for droplets that are positioned further from the boundary as the evaporation rates far away from the source are considerably smaller than near the source, as seen by the heat flux divergence in Fig. 11(c) and the differences in the PDF at $L = 0$ cm versus $L = 100$ cm in Fig. 11(a).

To simplify the problem and significantly reduce computational costs a prescribed PDF modeling is introduced. In this approach, the functional description of the PDF is parameterized by lower order moments, typically the mean and RMS. The degrees of freedom of the problem is reduced from the number of bins representing the PDF ($N = 30$) to just 2 (mean and RMS). In this study we explored this possibility by extracting the mean and RMS from the exact evolution PDF evolution and then used it to prescribe the entire PDF evolution using either an assumed Gaussian and log–normal distributions. Fig. 12(a) shows the time dependent arithmetic mean diameter (D_{mean}), the Sauter mean diameter (D_{32}), the root mean square RMS (σ_D) and skewness for the $M = 100$ μm, $S = 0.25$, $f_v = 1 \times 10^{-4}$ and $T_w = 1200$ K. D_{mean}, D_{32} and σ_D are observed to decrease with time while the skewness increases with time; consistent with previously observed skewed PDFs. D_{32} and σ_D for the calculations are used to prescribe a PDF assuming a log–normal distribution. Comparisons of the modeled PDF to the actual PDF are shown in Fig. 12(b). Overall the comparison is excellent. However, a similar comparison using a normal (Gaussian) distribution shown in Fig. 13 with $M = 100$ μm, $\sigma_D = 35$, $f_v = 1 \times 10^{-5}$ and $T_w = 1200$ K is not as successful. For the latter case, the assumed symmetry of the droplet PDF using the normal distribution introduces significant errors late in time after 10 s.

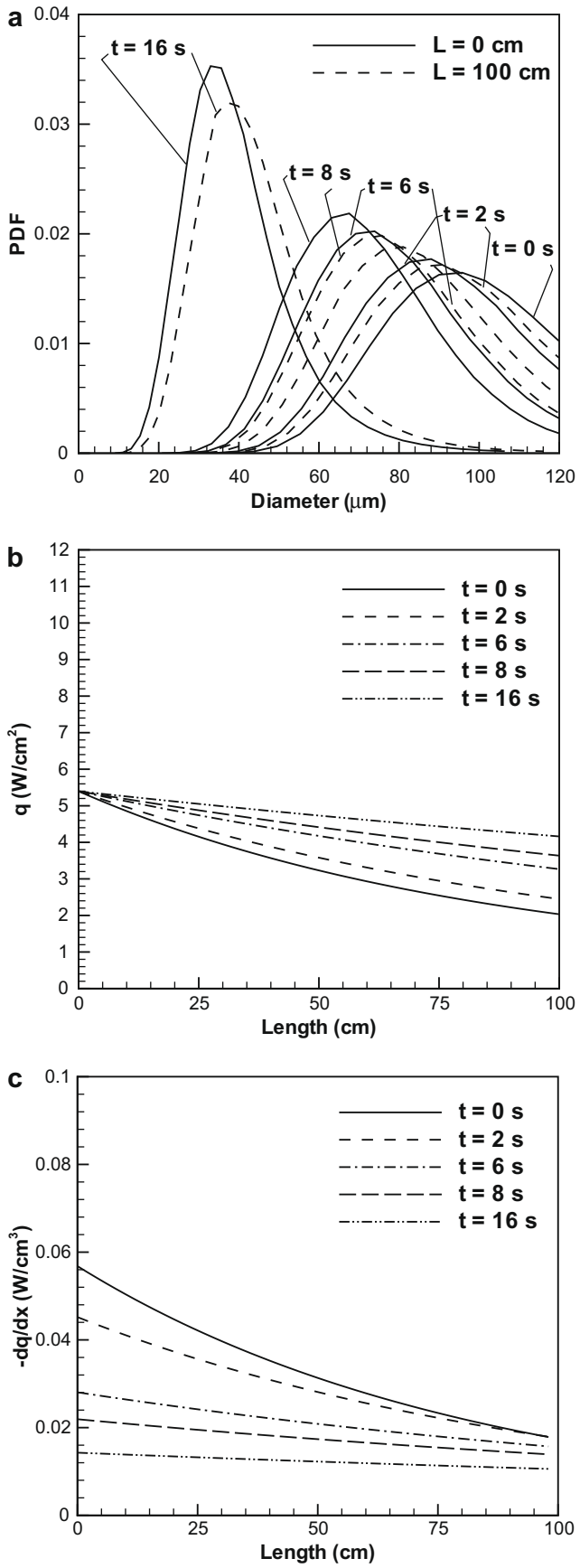

Fig. 10. Time evolution of (a) droplet size PDF, (b) radiative heat flux and (c) divergence of the radiative heat flux at $t = 0$ s, 2 s, 6 s, 8 s and 16 s for case $M = 100$ μm, $f_v = 10^{-5}$ and $T_{wall} = 1000$ K.

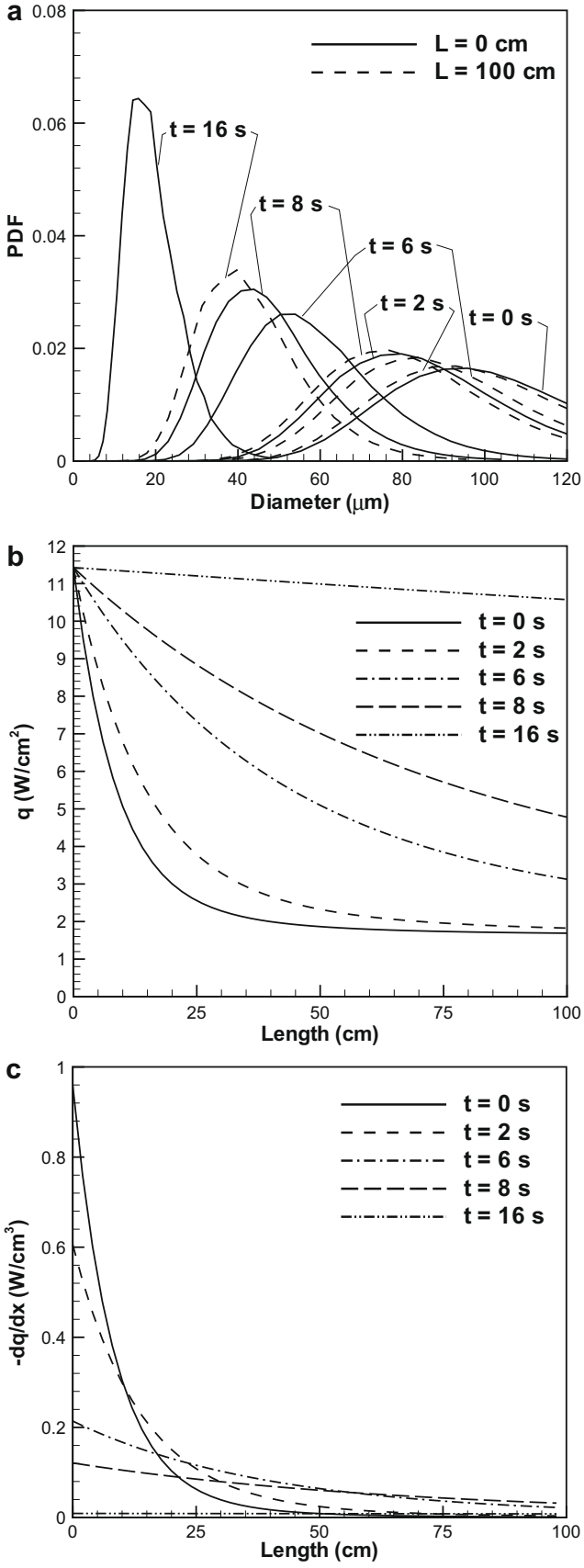

Fig. 11. Time evolution of (a) droplet size PDF, (b) radiative heat flux and (c) divergence of the radiative heat flux at $t = 0$ s, 2 s, 6 s, 8 s and 16 s for case $M = 100$ μm, $f_v = 10^{-4}$ and $T_{wall} = 1200$ K.

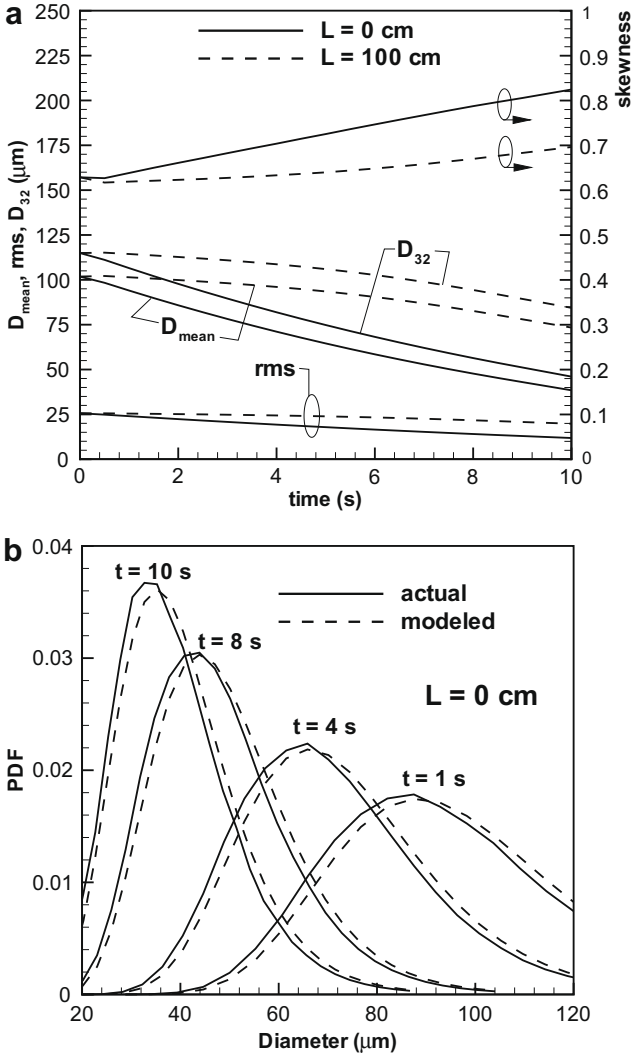

Fig. 12. Time evolution of the spray for an initial log–normal distribution with $M = 100$ μm, $S = 0.25$, $f_v = 1 \times 10^{-4}$ and $T_w = 1200$ K showing (a) arithmetic mean (D_{mean}), Sauter mean (D_{32}), RMS (σ_D) and skewness and (b) modeled PDF using lower order moments versus exact PDF.

These results show the importance of using a presumed PDF that can be asymmetric. The use of a prescribed PDF has several computational advantages. The reduced degrees of freedom characterizing the PDF evolution results in less equations to be solved (i.e., two moments versus many sections). In addition, the cost of evaluating droplet weighted radiative properties is tremendously reduced. As previously shown by the authors, significant savings can be achieved by Sauter mean scaling of the spray radiative properties [20]. The scaling procedure employees a non-linear interpolation to compute between radiative properties from precomputed tables and thereby avoids costly direct calculations from Mie theory. The precomputed tables however depend on a presumed functional form for the droplet PDF. Results from this study suggests that a distribution that accounts for skewness is required in order to attempt to describe the entire spray evolution by using a prescribed PDF in radiation driven evaporation problems.

5. Conclusions

A model for the evaporation of water sprays for 1D planar media is presented that uses a Lagrangian sectional description of the spray coupled with a full RTE solution for absorbing and scattering

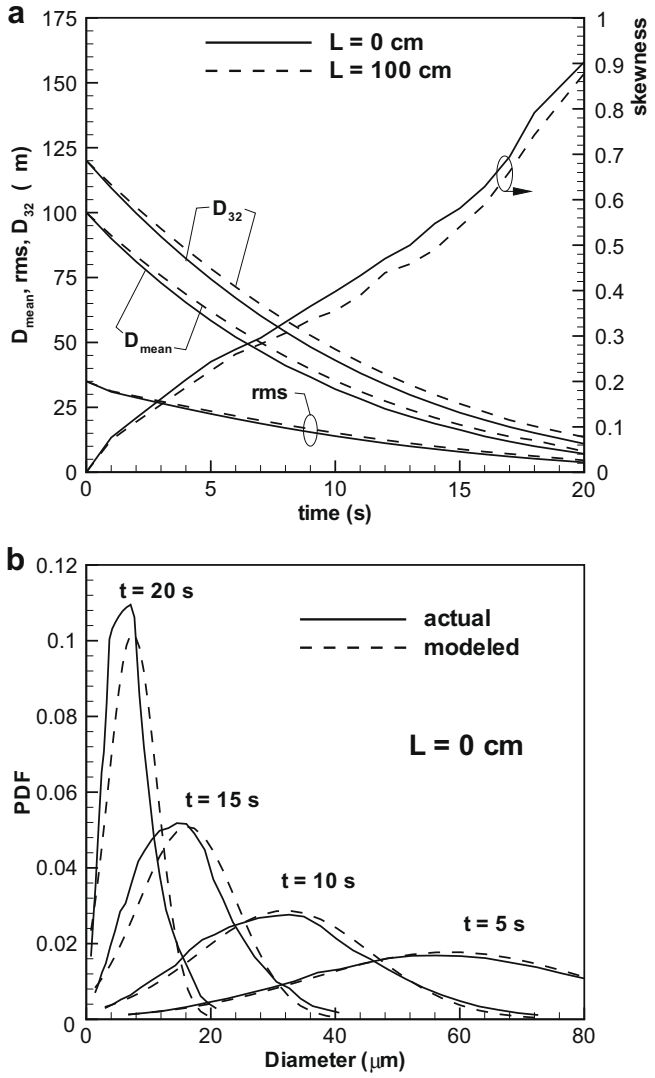

Fig. 13. Time evolution of the spray for an initial normal distribution with $M = 100\ \mu m$, $\sigma_D = 35$, $f_v = 1 \times 10^{-5}$ and $T_w = 1200$ K showing (a) arithmetic mean (D_{mean}), Sauter mean (D_{32}), RMS (σ_D) and skewness and (b) modeled PDF using lower order moments versus exact PDF.

media composed of water droplets and water vapor. The medium properties are calculated using Mie theory for the water droplets and the HITEMP database for the water vapor. The PDF of droplet size is shown to develop a positive skewness due to the decrease in absorption coefficient for small droplets. The existence of an optimal mean diameter that maximizes the spray absorption of radiate energy is observed. The optimum is a consequence of a trade-off between the increase in number density and decrease in droplet absorption efficiency with decreasing droplet size. Comparison of the droplet PDF compared to a modeled PDF revealed the importance of accounting for the positive skewness, therefore assumed distributions that enforce symmetry (e.g., a Gaussian distribution) will introduce error. It is expected that future efforts can take advantage of this fact to employ a Sauter mean scaling to efficiently evaluate radiative properties.

Acknowledgment

This research is supported by the National Science Foundation under Grant No. CTS-034811.

References

[1] J. Sacadura, Radiative transfer in fire safety science, J. Quant. Spectrosc. Radiat. Transfer 93 (2005) 5–24.
[2] F. Williams, On vaporization of mist by radiation, Int. J. Heat Mass Transfer 8 (1965) 575–587.
[3] G. Harpole, Radiative absorption by evaporating droplets, Int. J. Heat Mass Transfer 23 (1980) 17–26.
[4] P. Lage, R. Rangel, Single droplet vaporization including thermal radiation absorption, J. Thermophys. Heat Transfer 7 (1993) 502–509.
[5] P. Lage, R. Rangel, Total thermal radiation absorption by a single spherical droplet, J. Thermophys. Heat Transfer 7 (1993) 101–109.
[6] G. Miliauskas, Regularities of unsteady radiative–conductive heat transfer in evaporating semitransparent liquid droplets, Int. J. Heat Mass Transfer 44 (2001) 785–798.
[7] G. Miliauskas, Interaction of the transfer processes in semitransparent liquid droplets, Int. J. Heat Mass Transfer 46 (2003) 4119–4138.
[8] G. Miliauskas, Interaction of transfer processes during unsteady evaporation of water droplets, Int. J. Heat Mass Transfer 49 (2006) 1790–1803.
[9] L. Dombrovsky, Absorption of thermal radiation in large semi-transparent particles at arbitrary illumination of the polydisperse system, Int. J. Heat Mass Transfer 47 (2004) 5511–5522.
[10] C. Tseng, R. Viskanta, Enhancement of water droplet evaporation by radiation absorption, Fire Safety J. 41 (2006) 236–247.
[11] D. Sheppard, Spray characteristic of fire sprinklers, Ph.D. Dissertation, Northwestern University, Evanston, IL, 2002.
[12] J. Greenberg, I. Silverman, Y. Tambour, On the origins of spray sectional conservation equations, Combust. Flame 93 (1993) 90–96.
[13] W. Lentz, Generating Bessel functions in Mie scattering calculation using continued fractions, Appl. Opt. 15 (1976) 668–671.
[14] W. Wiscombe, Mie scattering calculations: advances in technique and fast, vector-speed computer codes, Tech. Rep. Technical Note, TN-140+STR, NCAR, 1979.
[15] L. Rothman et al., The HITRAN 2004 molecular spectroscopic database, J. Quant. Spectrosc. Radiat. Transfer 96 (2005) 139–204.
[16] M. Modest, R. Riazzi, Assembly of full spectrum k-distributions from a narrow-band database: effects of mixing gases and nongray absorbing particles and mixtures with nongray scatters in nongray enclosures, J. Quant. Spectrosc. Radiat. Transfer 90 (2005) 169–189.
[17] A. Wang, M. Modest, High-accuracy compact database of narrow-band k-distributions for water vapor and carbon dioxide, J. Quant. Spectrosc. Radiat. Transfer 93 (2005) 245–261.
[18] S. Kumar, A. Majumdar, C. Tien, The differential–discrete–ordinate method for solutions of the equation of radiative transfer, ASME J. Heat Transfer 112 (1990) 424–429.
[19] W. Fiveland, The selection of discrete ordinate quadrature sets for anisotropic scattering fundamentals of radiation heat transfer, ASME HTD 160 (1991) 89.
[20] W. Godoy, P. DesJardin, Efficient transmission calculations for polydisperse water sprays using spectral scaling, J. Quant. Spectrosc. Radiat. Transfer 108 (2007) 440–453.
[21] M. Modest, Radiative Heat Transfer, McGraw-Hill, Inc., New York, NY, 1993.
[22] C. Bohren, D. Huffman, Absorption and Scattering of Light by Small Particles, John Wiley & Sons, New York, NY, 1983.
[23] G. Hale, M. Querry, Optical constants of water in the 200-nm to 200-μm wavelength region, Appl. Opt. 12 (1973) 555–563.
[24] J. Barret, C. Clement, Growth and redistribution in a droplet cloud interacting with radiation, J. Aerosol. Sci. 21 (1990) 761–776.